Alternative thermal cycling treatment to produce abnormal grain growth in FeMnAlNi alloys:

study of composition variations and the effects on the relative phase stabilities

P. La Roca[a,b,c], L.M. Guerrero[b,d], A. Baruj[a,b], J.M. Vallejos[d,e], M. Sade*[a,b]

[a] Centro Atómico Bariloche and Instituto Balseiro, CNEA, Av. Bustillo 9500, San Carlos de Bariloche, Rio Negro, R8402AGP, Argentina

[b] Consejo Nacional de Investigaciones Científicas y Técnicas (CONICET), Argentina

[c] Institute for Advanced Materials (INAMAT), Universidad Pública de Navarra, Campus de Arrosadia, 31006 Pamplona, Spain

[d] Instituto de Física Rosario (CONICET-UNR), Bv. 27 de febrero 210 bis, Rosario, Santa Fe, Argentina

[e] Universidad Nacional del Nordeste, Facultad de Ingeniería, Las Heras 727, 3500 Resistencia, Argentina

* Corresponding author: sade@cab.cnea.gov.ar

Correspondence email: sade@cab.a.gov.ar

Abstract: An alternative method to obtain abnormal grain growth in Fe-Mn-Al-Ni system is presented. A crucible is used to control the cooling speed of the samples from 1200 ⁰C enabling the nucleation of the equilibrium fcc phase. This fcc structure leads to an abnormal grain growth after heating to 1200 ⁰C, temperature at which the bcc phase is stable. In this way, crystals with a mean diameter of 18 mm are obtained after 4 thermal cycles which take approximately 2 hours. Additionally, precise composition measurements using neutron activation allowed the detection of a decrease in Mn content after each thermal cycle. Using electrical resistivity measurements, the effect of the variation of Mn content on the relative phase stability between the bcc austenite and the fcc martensite has been observed and is discussed here.

Introduction

After the first report on the Au-Cd shape memory alloy in 1951 [1], several metallic systems showing the shape memory effect (SME) have been reported. Just as a few examples we mention CuAl, CuZnAl, CuAlNi, CuAlMn, NiTi, NiAl, FeMnSi [2]. Among the remarkable properties which these systems exhibit, the shape memory effect and pseudoelasticity are mainly studied and both properties are explained by the presence of a martensitic transformation. Pseudoelasticity is characterized by the large deformation obtained by applying mechanical forces at T >A_f (Austenite finish temperature) and the recovery of the original shape after unloading the material. This deformation usually called pseudoelastic deformation is several times larger than the allowed elastic deformation in metallic systems.

In 2011, a new pseudoelastic system based on Fe-Mn alloys was reported. This new thermoelastic system is a Fe-Mn-Al-Ni alloy with a large amount of Mn (equal or larger than 30 at.%) [3]. This remarkable result opened new scientific and technological possibilities since low cost Fe-based alloys showing thermoelasticity and pseudoelasticity could be developed by applying standard steelmaking techniques [4, 5]. The Fe-36Mn-15Al-7.5Ni (at. %) alloy shows an unusual martensitic transformation between a bcc austenitic structure (α) and a fcc martensite (γ') at temperatures close to room temperature [6], although this transition is not thermoelastic. A further addition of Ni and the introduction of nanometric precipitates, i.e., β NiAl phase with B2 order, lead to a thermoelastic martensitic transition [3]. Additionally, since the austenite becomes ferromagnetic and the martensite is antiferromagnetic, a strong change in magnetization takes place during the martensitic transformation, favoring the use of this system for the development of sensors [7, 8].

Another interesting property of this Fe-36Mn-15Al-7.5Ni (at. %) alloy is that the critical stress to transform shows a small variation with the temperature (0,5 MPa/°C). This property increases the temperature range for potential applications and leads to several advantages. For example, it allows the design of energy dissipation devices for the mitigation of natural or artificial vibrations in structures or machines subjected to relatively large temperature variations [3,4,9]. This slight dependence of the critical stress with temperature

is related to the entropy change between austenite and martensite, which is easily observed if the Clausius-Clapeyron equation is considered [2]. In the present case, it has been reported that the contribution of the magnetic entropy leads to a decrease of the entropy change between austenite and martensite [3].

Recently, it has been found that the addition of Cr to the FeMnAlNi alloy leads to a composition having a negligible entropy change. This property results in a pseudoelastic effect that is independent of temperature [10], a relevant result which further increases the useful temperature range and the potential technological use of the material [11].

An important point to consider here is the necessity of achieving specific microstructural characteristics in order to optimize the pseudoelastic properties of Fe-Mn-Al-Ni alloys [12-15]. In particular, precipitates must be introduced and large grains are necessary [12,16,17]. In fact, it has been shown that the bamboo-like microstructure favors the pseudoelastic effect and that mechanical reversibility increases for larger grain to sample size ratios [3,16]. After this finding, several techniques have been developed to obtain large grains. An example has been reported by Omori et al. [18]. These authors have shown that thermal cycling between 1200 ºC and a temperature in the range from 600 ºC to 700 ºC leads to an abnormal grain growth. In fact, after 10 of these thermal cycles, a grain size close to 30 mm is obtained [18, 19].

Vollmer et al. reported that abnormal grain growth is favored when Ti is added to Fe-Mn-Al-Ni due to the refinement of the subgrain size and that small amounts of Cr strongly inhibit the abnormal grain growth [20]. It is then possible to control the grain size by changing the chemical composition of the alloy. It is worth noticing that the polycrystalline material shows some aspects which limit the expected mechanical behavior. An example has been reported by Vollmer et al. [21]. These authors have shown that the orientation of the grains and the crystallographic compatibility among neighbor grains affect the mechanical reversibility, which decreases after mechanical cycling in alloys with bamboo microstructure [21]. On the other hand, pseudoelasticity reaches a large efficiency if single crystals are considered [15, 22, 23]. In this way, Vallejos et al. developed a method based on thermal cycling with a simultaneous directional annealing, which leads to single crystals after a short time interval [24-25].

This attractive scientific scenario leads to devote efforts to explore different methods either to obtain large grains or to produce single crystals. Omori et al. have reported that thermal cycling between convenient selected temperatures in Fe-Mn-Al-Ni alloys affects the amount of the equilibrium fcc phase (γ) in the (α + γ) two phase region, being the amount of γ closely related to the final grain size [18]. These authors use a thermal cycling treatment between 600 ºC and 1100 °C.

The present manuscript presents and analyzes a rather simple method which controls the cooling speed of the Fe-Mn-Al-Ni alloy from 1200 ºC using a large mass crucible which wraps up the material, thus imposing the sample temperature. In this way, a large amount of γ phase is obtained which favors abnormal grain growth after heating back to 1200 ºC. After repeating this procedure only 4 times large grain sizes are obtained. This procedure also leads to variations of composition due to the Mn evaporation. These variations are also measured by a precise neutron activation technique and finally the effect of these variations on the relative phase stability between austenite and martensite is analyzed. In what follows, we will use the symbol γ for the fcc structure which is stable in the temperature range from 600ºC to 1150º C, α for the metastable retained bcc structures after quenching from 1200 ºC and γ' for the fcc martensite which forms at temperatures close to room temperature.

Experimental method

A Fe-Mn$_{36}$-Al$_{15}$-Ni$_{7.5}$ alloy was prepared by arc melting pure metals (99.98 at. %) seven times under Ar atmosphere. A 15 g alloy button was obtained and then heat treated in quartz tubes under Ar atmosphere during 48 hours at 1000 ºC. The obtained material was then water quenched by breaking the capsule. After this, the button was hot rolled at 1000 ºC down to a thin plate of 1 mm thickness. This procedure was performed through several steps keeping the deformation below the limit of 15% in each individual pass. Samples (1x5x35 mm^3) were then obtained by spark cutting the plate as illustrated in Fig.1a and were named S0, S1, S2, S3 and S4. The name of the samples

indicated the number of thermal cycles to be performed and were randomly assigned in order to avoid effects of possible directional composition inhomogeneities.

A 750 g Fe-Mn-Si block was divided in two parts and a bed was machined with parallel sides of 35 mm x 30 mm x 100 mm. The other part was also machined to serve as a cover for the flat surface. The block was used as a crucible in the high temperature thermal treatments performed to the samples, in an attempt to minimize the effect of Mn loss. Samples S0 to S4 were placed on the block bed and covered by the second part of the block. The crucible was then introduced in a furnace chamber at 1200 ºC for 20 min. Sample S0 was quenched in water at room temperature after this first treatment. Afterwards, samples S1 to S4 were submitted to a different number of steps in a similar cyclic heat treatment as described below and schematically shown in Fig.1c. Samples S1 to S4 were let to cool down inside the block for 10 min after it was taken out of the furnace, as shown in Fig. 1b. Sample S1 was taken out of the crucible (point A in Fig.1c). The crucible with the rest of the samples was introduced again in the furnace chamber and the procedure was repeated for the other samples as described in Fig.1c, leading to an incremental number of thermal cycles for each sample. Samples S2, S3 and S4 were taken out from the crucible after the following 10 minutes cooling steps (point B, C and D in Fig.1c). Finally, samples S1 to S4 were laid in the crucible bed which was introduced again in the furnace chamber at 1200 ºC for 20 minutes and subsequently quenched in water at room temperature. In this way, each sample was submitted to a different number of thermal cycles. The sample identified as SII in Fig. 1c corresponds to a small piece that was let to cool down slowly inside the crucible and taken out from the crucible at point B of the figure for observation purposes.

All thermally treated samples were mechanically polished to a thickness of 0.7 mm, removing the superficial oxide layer. Then, the samples were chemically polished in Nital 3% (3% vol. nitric acid in ethylic alcohol) during time intervals in the range from 20 seconds to 2 minutes and the surface of each sample was optically analyzed using an Olimpus Optical Microscope. The grain size was measured by the intersection method. In all cases the obtained and reported values correspond to

the average of several measurements in each sample, using the standard deviation to determine the error of the measurement. In those cases, where the grain size was large, only a few grains could be intersected in each individual measurement. Grains in sample S4 were big enough to be easily noticed with the naked eye. In this case, standard photographs were used to measure the grain size instead of the Olimpus microscope.

The composition of each sample was determined using a high precision neutron activation technique in the RA-6 nuclear reactor located at Centro Atómico Bariloche, as described in refs. [26, 27, 28]. The martensitic transformation was analyzed using electrical resistivity measurements in a non-commercial equipment, with cooling and heating speeds equal to 10 K/min. After this, samples were polished down to 0.2 mm thickness and 3 mm in diameter disks were cut by spark-erosion for transmission electron microscopy (TEM). These discs were electrochemically polished by using a double jet technique with an acetic-perchloric solution 95:5. Finally, these samples were observed in a Philips CM200 TEM with an accelerating voltage of 200 kV and Ultratwin objective lens.
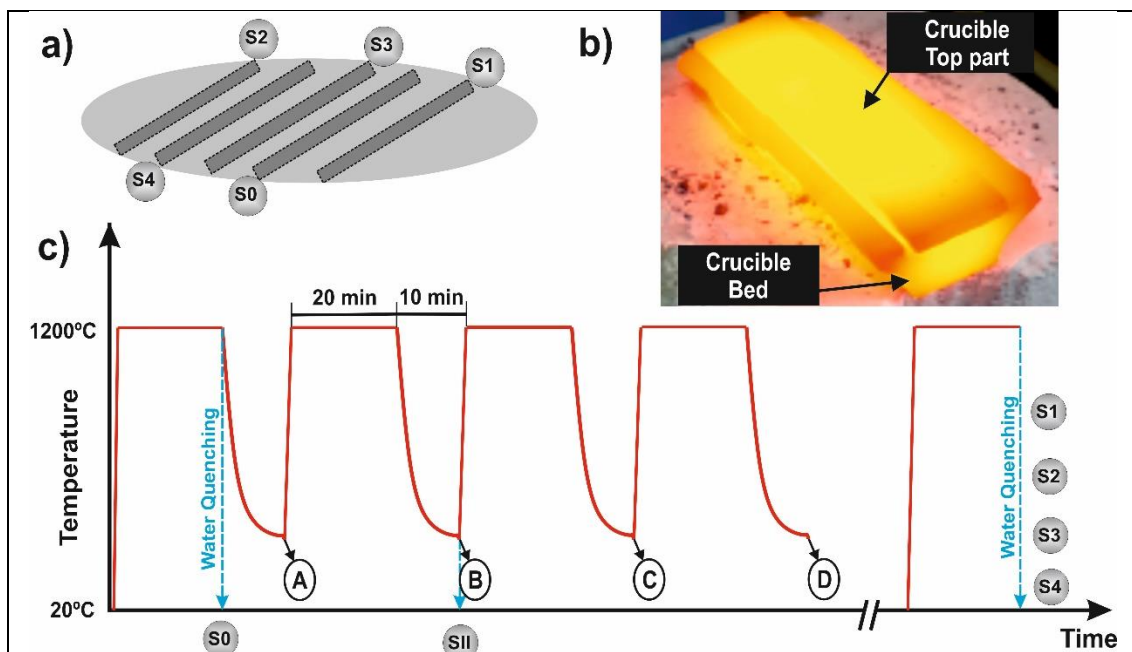

Figure 1: Performed procedure to obtain abnormal growth. a) Samples were obtained from a hot rolled plate of Fe-Mn$_{36}$-Al$_{15}$-Ni$_{7.5}$ alloy; b) Fe-Mn-Si crucible used for the thermal treatment of samples S0 to S4; and c) Temperature vs. time for the reference sample S0 and for thermal cycles performed on samples S1 to S4. Points A,B,C and D indicate when samples S1,S2,S3 and S4 are taken out from the crucible respectively. Samples S1 to S4 are finally taken back in the crucible for 20

minutes aging at 1200 °C and finally quenched in water as indicated by the vertical dot line at the right side of the figure.

Results and discussion

In order to characterize the thermal behavior of the crucible used for the cyclic treatment, the variation of its temperature as a function of time was measured after taking it out of the furnace chamber at 1200 ⁰C. The temperature was measured after 5 min,10 min and 30 min with a thermocouple attached to it. The obtained data are shown in Fig. 2a. An exponential decay function correctly fits the obtained results, following the Newton cooling behavior. It can be observed that after the first 10 min at room temperature, the temperature reaches approx. 240 ⁰C (Fig.1c). It is expected that this time interval should be enough to allow the nucleation and growth of a required amount of the γ phase. Longer cooling time intervals would not favor a larger amount of γ phase due to the strong decrease of diffusion mechanisms with temperature. Shorter time intervals might decrease the amount of the γ phase.

With the purpose of quantifying the amount of the formed γ phase, a small piece (SII) was analyzed after the second 10 minutes cooling step (see point B in Fig.1c). Fig. 2b shows the obtained microstructure. The γ phase can be observed in violet color, obtained by using polarized light in the optical microscope, with its typical morphology [18]. Using the ratio between the areas representing the α phase (in black, in Fig.2b) and the γ phase (in violet, in Fig.2b), it could be estimated that the amount of γ reaches an amount of approximately 81%, close to the amount reported by Omori et al. [18] after thermal cycles in the temperature range from 600⁰ to 1000 ⁰C. These authors report that larger fractions of γ phase, obtained before annealing at 1200 ⁰C, favor the abnormal grain growth. It is then expected that the thermal treatment proposed in the present manuscript, which produces large fractions of γ phase before ageing at 1200 ⁰C, could yield positive results concerning abnormal grain growth.
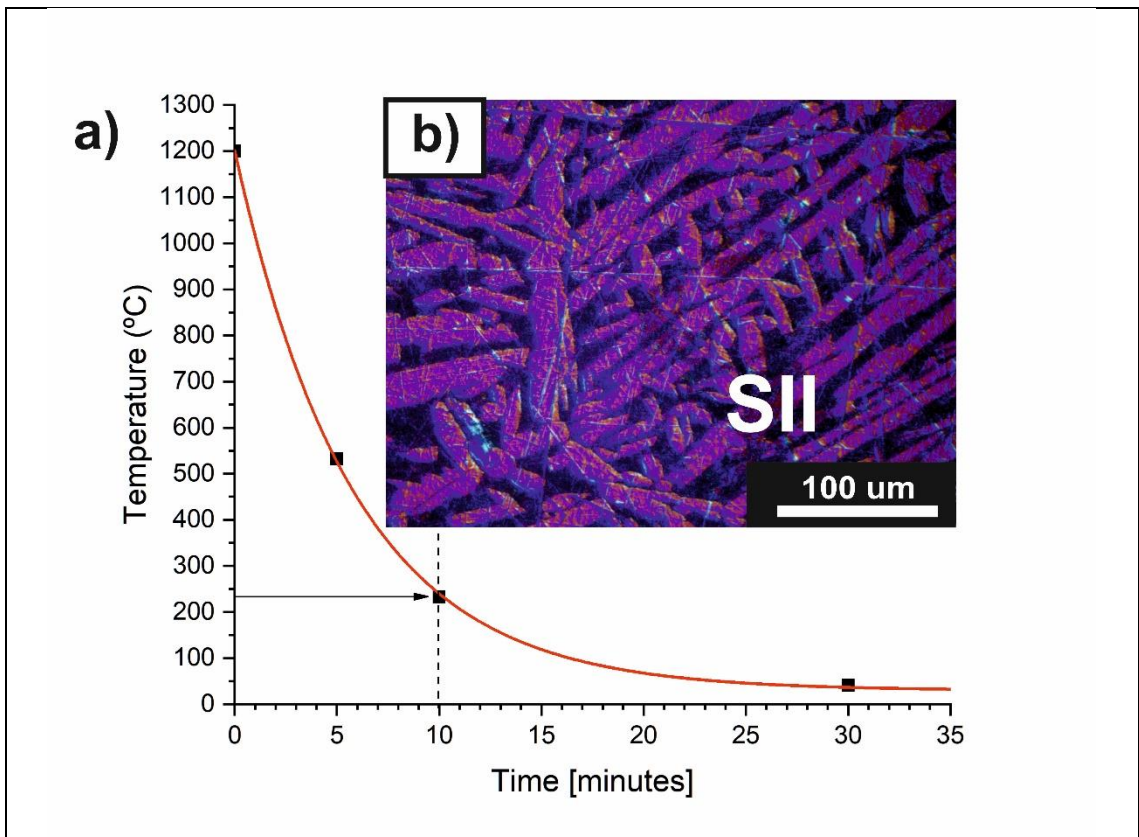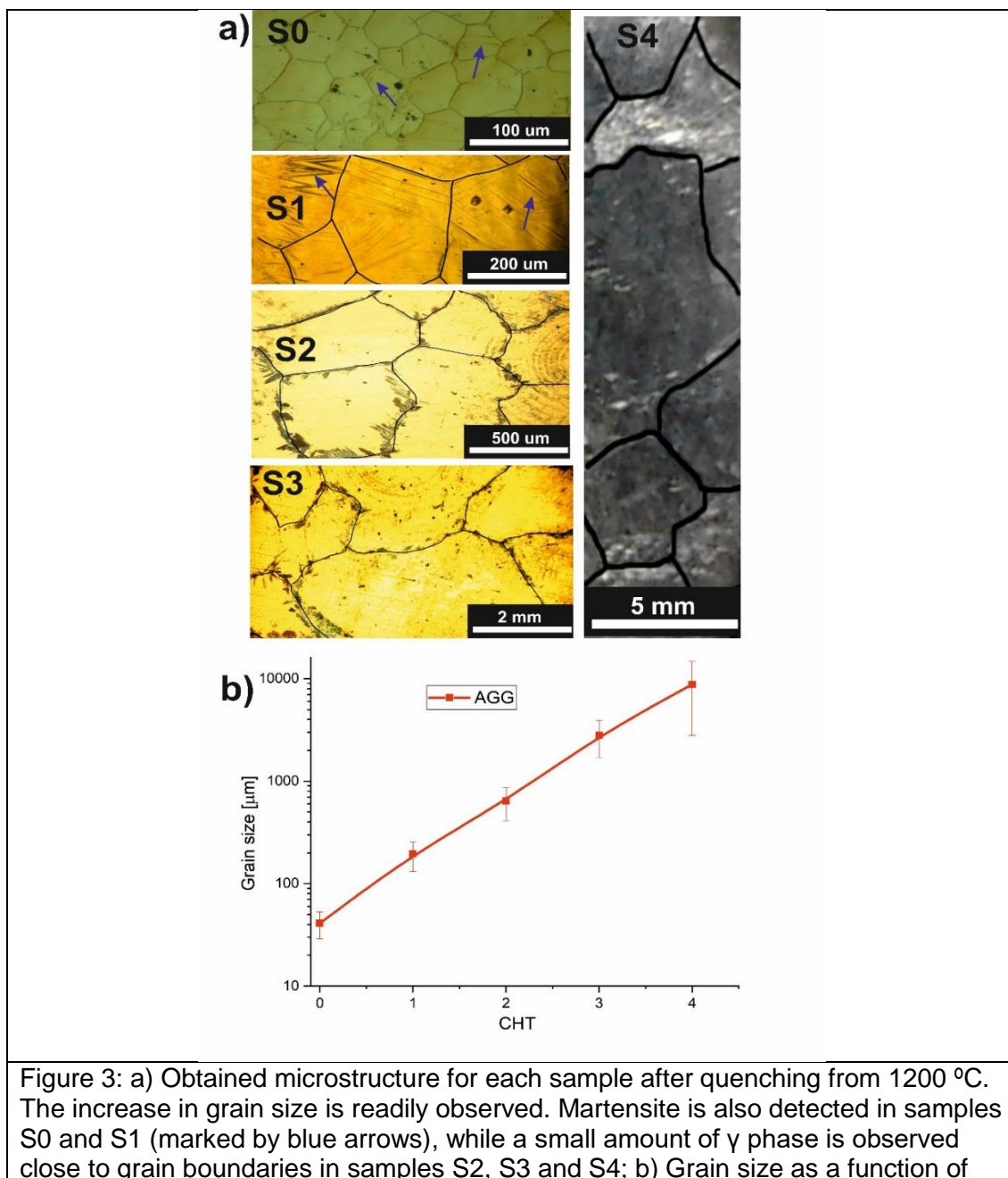
Figure 2: a) Temperature vs. time measurement obtained for the empty crucible after taking it from the furnace chamber at 1200 ºC and b) Microstructure obtained by optical microscopy for sample SII (Fig.1c). Violet and black colors correspond to γ and α phases, respectively.

Fig.3a shows the obtained microstructure for samples S0 to S4 after quenching from 1200 ºC. The contrast of grain boundaries was enhanced to help the eye. The grain size progressively increases from 40 μm in sample S0 up to 18 mm in sample S4. Fig. 3b shows the evolution of grain size as a function of the number of thermal cycles. The applied cyclic treatment is clearly an efficient way to obtain an abnormal grain growth. It could also be a potential mechanism to get single crystals using a single furnace and conventional methods.

Some γ´ martensite plates appeared in samples S0 and S1 (marked by blue arrows in Fig. 3a). In samples S2, S3 and S4, no martensite was detected and the presence of the stable γ phase was

detected close to the grain boundaries, although in small amounts which might not significantly affect the material properties. <mark>According to Vollmer et al. [29],</mark> the presence of γ phase at the grain boundaries could be related to the quenching speed from 1200 °C which might probably be not sufficiently high. However, all samples used here have the same geometry and were quenched simultaneously with the same procedure. It is also possible to rationalize the presence of γ and γ' with variations in composition originated in the thermal treatment of each sample, a possibility that will be analyzed below.

Figure 3: a) Obtained microstructure for each sample after quenching from 1200 °C. The increase in grain size is readily observed. Martensite is also detected in samples S0 and S1 (marked by blue arrows), while a small amount of γ phase is observed close to grain boundaries in samples S2, S3 and S4; b) Grain size as a function of

number of thermal cycles between 1200 ºC and 240 ºC obtained by taking the crucible out of the furnace chamber during 10 minutes and taking it back to the same chamber at 1200 ºC.

Fig.4 shows the electrical resistivity vs. temperature curves obtained for all quenched samples. These curves show the typical hysteresis of the α-γ´ martensitic transformation and a slope change associated to the magnetic ordering of the α phase. The morphology of the curve corresponding to the S0 sample is similar to the one reported in the literature [14]. However, it is not possible to precisely determine the martensitic critical transformation temperatures, although it is remarkable that the performed cyclic heat treatment leads to a decrease of the thermal hysteresis and to a shift of the whole cycles to lower temperatures. As the thermal cycling proceeds, the martensitic transformation is increasingly hampered. This effect might be related to an increasing stability of the α austenite. This result is consistent with the presence of γ´ plates in samples S0 and S1 and the absence of that phase in samples S2 to S4 (Fig. 4). Moreover, no hysteresis was detected for sample S4 in the whole measured temperature range down to -150 ºC. This indicates that the martensitic transformation did not take place due to an increase in the barriers which oppose the structural transition [13]. Another factor which might affect the relative phase stability is the grain size which strongly varies in the analyzed samples. However, as it has been shown in several Fe-Mn alloys, this effect becomes noticeable when the grain size is smaller than 30 µm [30, 31]. Additionally, the decrease in grain size has been shown to affect the martensitic transformation in an opposite direction to the one detected here, since for smaller grain sizes, the energetic barrier opposing the transformation, increases leading to the stabilization of the austenite [31]. Due to these reasons we can expect that composition changes originated in the evaporation of one of the components might explain the effects related to changes in the relative phase stability, as it will be discussed below.
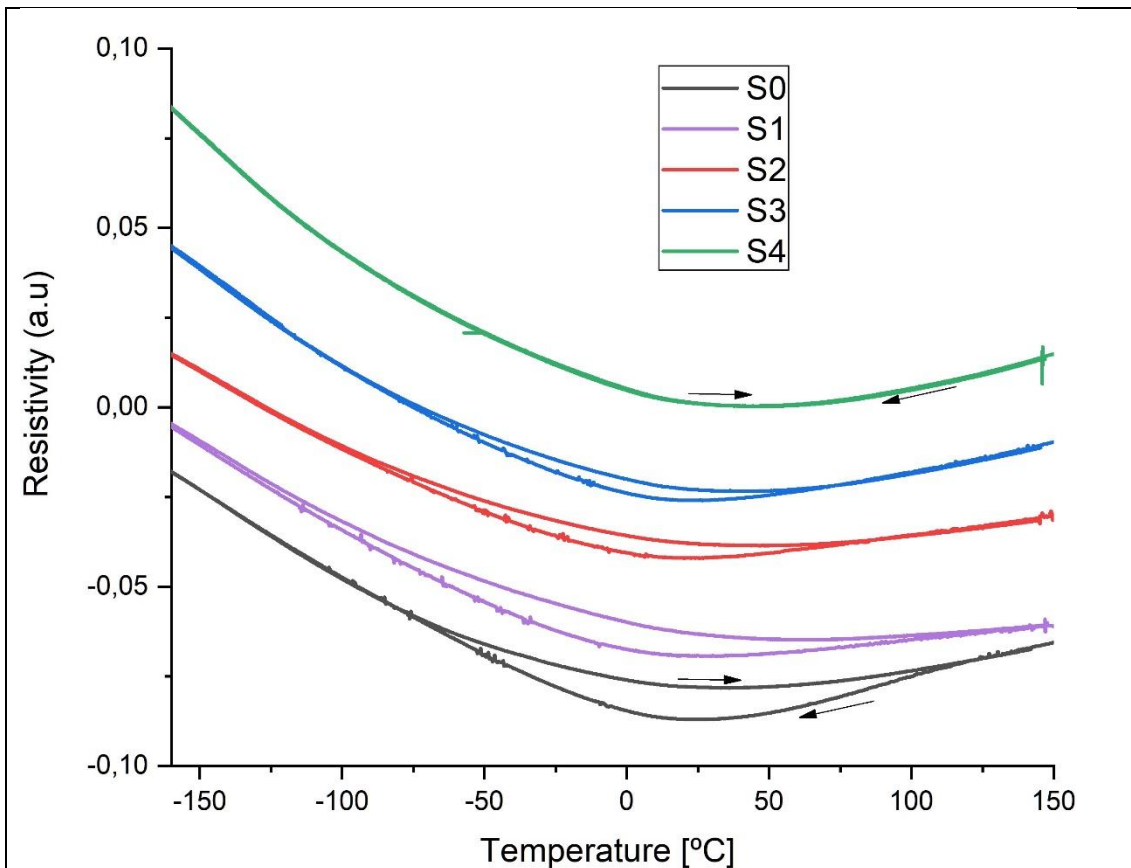
Figure 4: Electrical resistivity vs. temperature curves for all samples used in this work. No hysteresis is detected for sample S4 indicating the absence of the martensitic transformation. Thermal hysteresis is detected for samples S0 to S3 and it is noticeable that as grain size increases thermal hysteresis decreases and the whole cycle shifts to lower temperatures.

Fig.5 shows the evolution of the chemical composition as a function of time. In this case, the time variable corresponds to the interval where the samples stay at high temperature i.e., 30 min for each thermal cycle as shown in Fig.1. The inset in this figure shows a table with the compositions measured for each sample. A decrease in Mn is observed as the number of cycles increases, which is reasonable considering the tendency of Mn to evaporate at high temperatures due to its high vapor pressure [32]. As a related consequence, it can be observed an increase in the relative content of the other components, which is consistent with a loss of Mn atoms only. It is relevant to mention that due to the high resolution of the neutron activation technique used for the composition measurement, the detected variations are larger than the experimental errors. It is also noticed that before each measurement, the oxide layer of the surface was eliminated. This result is relevant since, in order to get good pseudoelastic properties in these alloys, thermal treatments at high

temperatures are required to increase the grain size. Additionally, considering the nature of this phenomenon, it is expected that it will show a more intense effect for samples with larger surface to volume ratios.
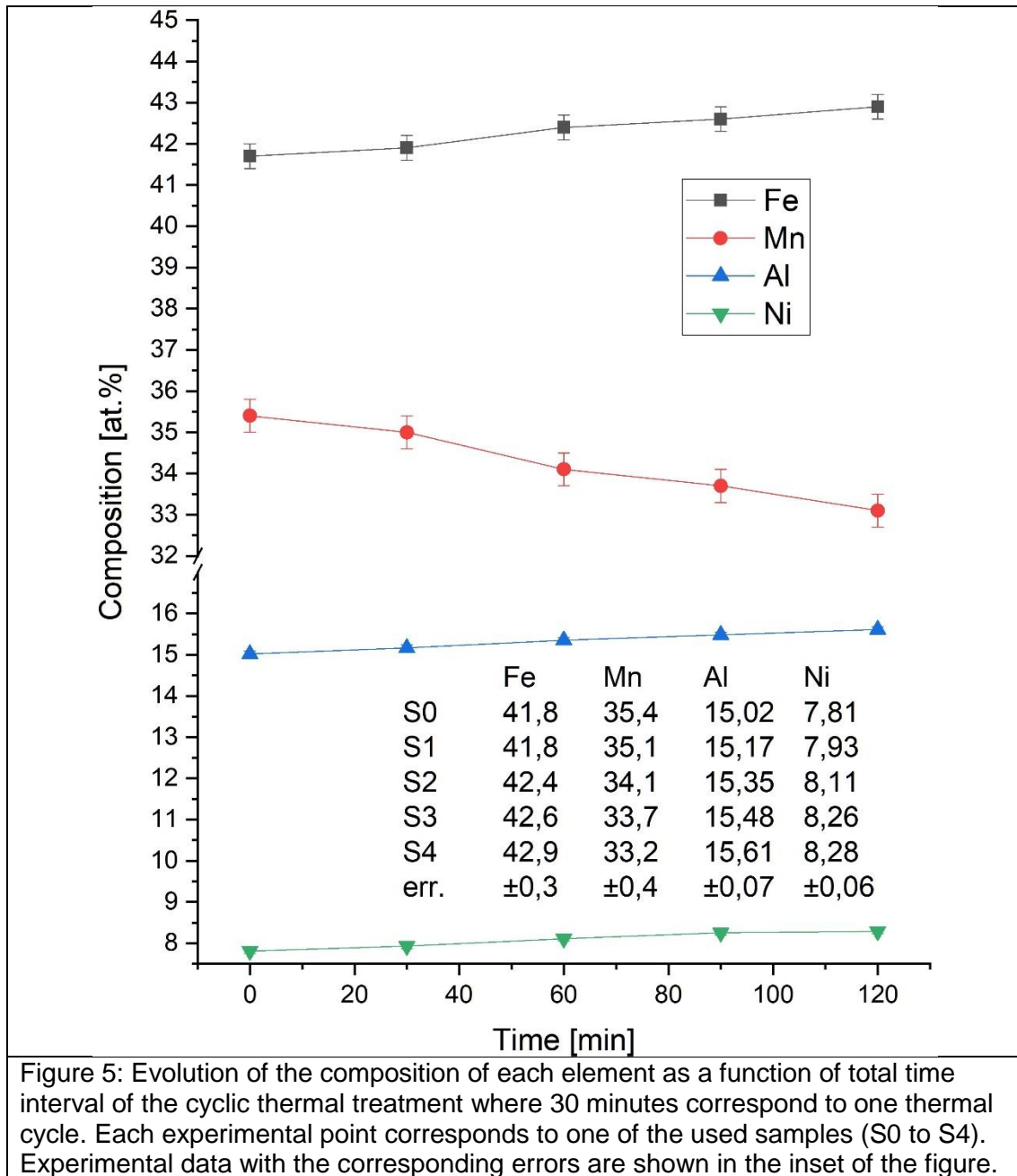

	Fe	Mn	Al	Ni
S0	41,8	35,4	15,02	7,81
S1	41,8	35,1	15,17	7,93
S2	42,4	34,1	15,35	8,11
S3	42,6	33,7	15,48	8,26
S4	42,9	33,2	15,61	8,28
err.	±0,3	±0,4	±0,07	±0,06

Figure 5: Evolution of the composition of each element as a function of total time interval of the cyclic thermal treatment where 30 minutes correspond to one thermal cycle. Each experimental point corresponds to one of the used samples (S0 to S4). Experimental data with the corresponding errors are shown in the inset of the figure.

As shown in Fig.4 a shift of the curves corresponding to the thermally induced martensitic transformation is observed as the thermal treatment includes more cycles (S0 to S4). This effect can be analyzed considering the measured composition variations (Fig.5) as follows:

1) Considering the phase diagram reported for this alloy system it can be deduced that an evaporation of Mn would lead to an increase in the martensitic transformation temperatures [3, 33].

2) The evaporation of Mn leads to an increase in the content of Al and Ni. Both elements contribute to the formation of nanoprecipitates. This might promote a decrease in the martensitic transformation temperature, enabling the presence of thermoelasticity and pseudoelasticity as well [13, 33].

3) An increase in the density of precipitates rich in Al and Ni leads to an increase in the Mn content of the matrix. As it has been shown by Walnsch et al., an increase in Mn in the bcc austenite leads to a decrease in the martensitic transformation temperature [33]. In addition, the precipitation of the B2 phase produces the stabilization of the austenitic state from a thermodynamical point of view [33]. These authors proposed that the α→γ' martensitic transformation is accompanied with the simultaneous transformation of the B2 precipitates into a tetragonal L_{10} phase. The driving force required to produce the latter transformation is several times larger than the one needed for the α→γ' transformation. As a consequence, if there were a larger volume fraction of precipitates in the α matrix, the M_S would be lower since a greater overcooling would be required to produce both transformations.

Considering the mentioned effects, it is expected that the decrease in the stability of the fcc γ' martensite is mainly a consequence of the relative increase in Ni and Al contents which would favor the nucleation and growth of precipitates. This has been confirmed by transmission electron microscopy observations which show the presence and the increased of density and size of precipitates in sample S4 in comparison with sample S0. Dark field TEM images of the microstructures of both samples are shown in Fig. 6. The effect of these precipitates on the relative phase stability can be explained in terms of two factors:

i) An increase in the number and size of precipitates increases the energy barrier that opposes to the transformation. This increased energy barrier, considered as elastic, leads to a decrease of the martensitic transformation temperatures [13].

ii) The nucleation and growth of precipitates also contribute to the composition variation of the matrix, i.e., an increased Mn content of the matrix, which also leads to a decrease in the martensitic transformation temperatures [33].

Both mentioned factors might contribute to the observed changes in the martensitic transformation cycle (Fig. 4). In order to find out the exact contribution of each effect, more research would be necessary. Another point for future research would be to characterize the effect of the obtained grain growth on the pseudoelastic properties of the material. Finally, an interesting point to consider is that nanoprecipitates which were introduced after aging at 200 ºC [3,12, 13, 15] have been introduced in the present work with a high-volume fraction and homogeneous distribution by the thermomechanical treatment used to get an abnormal grain growth. It is then possible to use the controlled variation of the global Mn content as an additional parameter to optimize the microstructure of the present Fe-Mn-based alloys.

The results shown in the present work also highlight the importance of controlling the chemical composition of the alloy. As recently reported, small changes in the composition seem to dramatically affect the pseudoelastic behavior [10, 11, 23] and grain growth rate [20, 34] in this system.
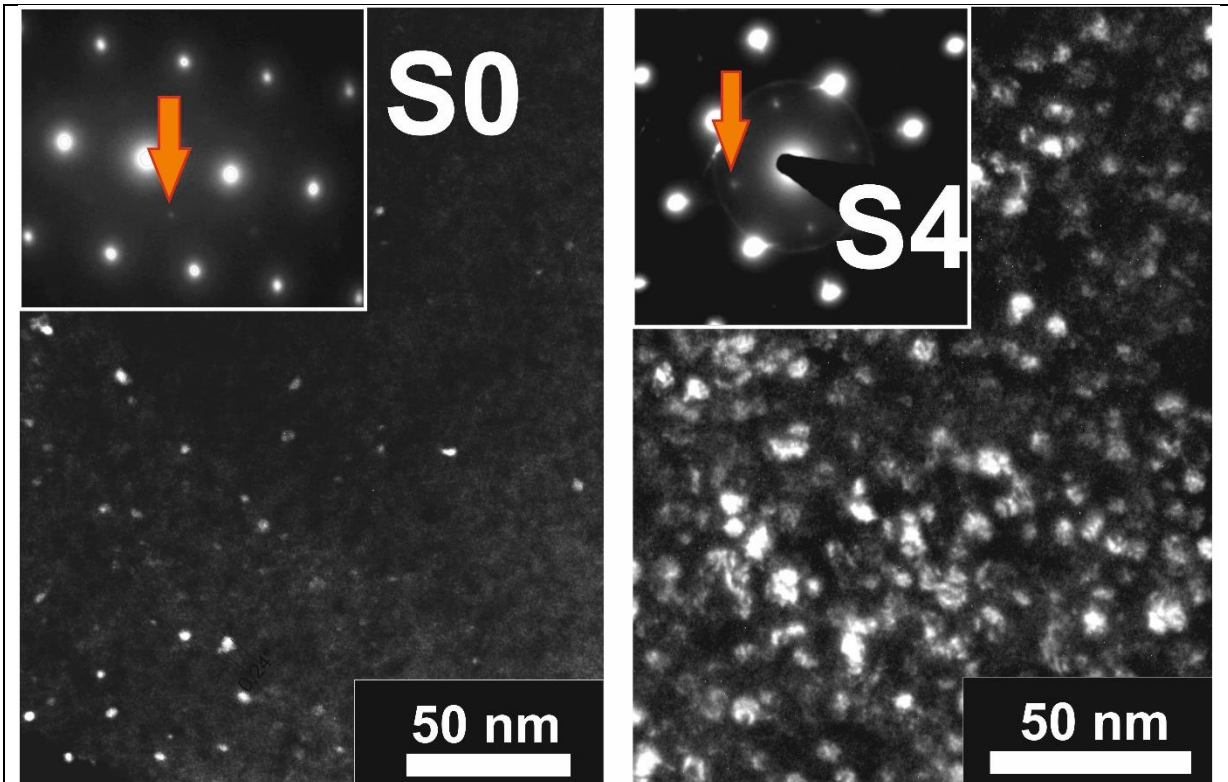
Figure 6: Dark field TEM images of samples S0 and S4 (Zone axes close to $[200]_\alpha$). A strong increase in density and size of precipitates is observed in sample S4 in comparison with S0.

Conclusions

- A method to obtain abnormal growth through the nucleation and growth of fcc γ phase was developed and optimized.

- The method increases the stability of the bcc austenite leading to a decrease of the martensitic transformation temperatures.

- Results are rationalized considering the evaporation of Mn and the related relative increase of Al and Ni contents.

- Nucleation and growth of precipitates are favored by the obtained composition variations which can be controlled by the present method.

- Precipitates are formed, which on one hand increase an elastic barrier to the martensitic transformation and on the other hand affect this transition in the same direction due to the corresponding variation of Mn content in the bcc matrix austenite.

Acknowledgments

References.

[1] L.C. Chang, T. A. Read, Plastic Deformation and Diffusionless Phase Changes in Metals-The Gold Cadmium Beta Phase. Trans. Am. Inst. Met. Eng. 189 (1951) 47.

[2] "Shape Memory Materials", Ed.: K. Otsuka, C.M. Wayman. Cambridge University Press (1998).

[3] T. Omori, K. Ando, M. Okano, X. Xu, Y. Tanaka, I. Ohnuma, R. Kainuma, K. Ishida, Superelastic Effect in Polycrystalline Ferrous Alloys, Science 333 (2011) 68-71.

[4] W. Abuzaid, Y. Wu, R. Sidharth, F. Brenne, S. Alkan, M. Vollmer, P. Krooß, T. Niendorf & H. Sehitoglu, FeMnNiAl iron-based shape memory alloy: promises and challenges. Shap. Mem. Superelast. 5 (2019) 263–277.

[5] P. La Roca, A. Baruj, M. Sade, Shape-memory effect and pseudoelasticity in Fe–Mn-based alloys. Shap. Mem. Superelasticity 3 (2016), 37-48.

[6] K. Ando, T. Omori, I. Ohnuma, R. Kainuma, K. Ishida, Ferromagnetic to weak-magnetic transition accompanied by bcc to fcc transformation in Fe–Mn–Al alloy. App. Phys. Lett. 95 (2009) 212504.

[7] H. Ozcan, J. Ma, J.E. Schaffer, I. Karaman, Large Dimension and Low-Cost Fe-SMA Rods. MATEC Web of Conf. 271, 01005 (2019).

[8] N. Malone, P. Miller, H. Ozcan, J. Ma, J. Schaffer, I. Karaman, Integrated Health Monitoring of Transportation Structures with Magnetic Fe-SMA Wires. MATEC Web of Conf. 271 (2019) 01008.

[9] M. Popa, B. Pricop, R-I. Comaneci, G. Gurau, M. Vollmer, P. Krooss, T. Niendorf, L-G. Bujoreanu, Processing effects on tensile superelastic behaviour of Fe43.5Mn34Al15±XNi7.5±X shape memory alloys. ModTech2019, Mater. Sci. Eng. 591 (2019) 012026.

[10] J. Xia, Y. Noguchi, X. Xu, T. Odaira, Y. Kimura, M. Nagasako, T. Omori, R. Kainuma, "Iron-based superelastic alloys with near-constant critical stress temperature dependence", Science 369, I 6505, 855-858 (2020).

[11] P. La Roca, M. Sade, Science, "Designing a wider superelastic window", 369 ISSUE 6505, 773-774 (2020). https://doi.org/10.1126/science.abc8244.

[12] T. Omori, M. Nagasako, M. Okano, K. Endo, R. Kainuma, Microstructure and martensitic transformation in the Fe-Mn-Al-Ni shape memory alloy with B2-type coherent fine particles. App. Phys. Lett. 101 (2012) 231907.

[13] P. La Roca, A. Baruj, C. Sobrero, J. Malarria, M. Sade, Nanoprecipitation effects on phase stability of Fe-Mn-Al-Ni alloys. J. Alloys Compd., 708 (2017) 422-427.

[14] P. La Roca, J. Medina, A. Baruj, C. Sobrero, M. Avalos J. Malarria, M. Sade, "Effects of B2 nanoprecipitates on the phase stability and pseudoelastic behavior of Fe-Mn-Al-Ni shape memory alloys", MATEC Web of Conferences 33:04005 (2015).

[15] L.W. Tseng, J. Ma, B.C. Hornbuckle, I. Karaman, G.B. Thompson, Z.P. Lou, Y.I. Chumlyakov, The effect of precipitates on the superelastic response of [1 0 0] oriented FeMnAlNi single crystals under compression. Acta Mater. 97 (2015) 234-244.

[16] T. Omori, M. Okano, R. Kainuma, Effect of grain size on superelasticity in Fe-Mn-Al-Ni shape memory alloy wire. APL Materials 1 (2013) 032103.

[17] H. Ozcan, Ji Ma, S.J. Wang, I. Karaman, Y. Chumlyakov, J. Brownd, R.D. Noebe, Effects of cyclic heat treatment and aging on superelasticity in oligocrystalline Fe-Mn-Al-Ni shape memory alloy wires. Scripta Mater. 134 (2017) 66–70.

[18] T. Omori, H. Iwazako, R. Kainuma, Abnormal grain growth induced by cyclic heat treatment in Fe-Mn-Al-Ni superelastic alloy. Mater. Des. 101 (2016) 263-269.

[19] T. Kusama, T. Omori, T. Saito, S. Kise, T. Tanaka, Y. Araki, R. Kainuma, Ultra-large single crystals by abnormal grain growth. Nature Comm 8 (2017) 354.

[20] M. Vollmer, T. Arold, M. J. Kriegel, V. Klemm, S. Degener, J. Freudenberger, T. Niendorf, Promoting abnormal grain growth in Fe-based shape memory alloys through compositional adjustments. Nature Comm. 10 (2019) 2337.

[21] M. Vollmer, P. Kroob, M.J. Kriegel, V. Klemm, C. Somsen, H, Ozcan, I. Karaman, A. Weidner, D, Rafaja, H. Biermann, T. Niendorf, Cyclic degradation in bamboo-like Fe-Mn-Al-Ni shape memory alloys-The role of grain orientation. Scr. Mater. 114 (2016) 156-160.

[22] L.W. Tseng, Ji Ma, S.J. Wang, I. Karaman, Y.I. Chumlyakov, Effects of crystallographic orientation on the superelastic response of FeMnAlNi single crystals. Scr. Mater. 116 (2016) 147-151.

[23] J.M Vallejos, M.F. Giordana, C.E. Sobrero, J.A. Malarria, Excellent pseudoelasticity of Al-rich Fe–33Mn–17Al–6Ni–0.15C (at%) shape memory single crystals obtained without an aging conditioning stage. Scr. Mater. 179 (2020) 25-29.

[24] J.M. Vallejos, M.E. Leonard, C.E. Sobrero, P.M. La Roca, A.V. Druker, J.A. Malarria, Design, construction, and performance of a device for directional recrystallization of metallic alloys. Rev. Sci. Instrum. 88 (2017) 025107.

[25] J.M. Vallejos, J. Malarria, Growing Fe-Mn-Al-Ni single crystals by combining directional annealing and thermal cycling. J. Mat. Proc. Tech. 275 (2020) 116317.

[26] S. Cotes, M. Sade, A. Fernández Guillermet, Fcc/hcp martensitic transformation in the Fe-Mn system: experimental study and thermodynamic analysis of phase stabilities, Metall. Trans. 26A (1995) 1957–1969.

[27] L. Guerrero, P. La Roca, F. Malamud, A. Baruj, M. Sade, Composition effects on the fcc-hcp martensitic transformation and on the magnetic ordering of the fcc structure in Fe-Mn-Cr alloys. Mater. Des. 116 (2017) 127-135.

[28] P. La Roca, P. Marinelli, A. Baruj, M. Sade, A.F. Guillermet, Composition dependence of the Néel temperature and the entropy of the magnetic transition in the fcc phase of Fe-Mn and Fe-Mn-Co alloys. J. Alloys. Compd. 688 (2016) 594-598.

[29] M. Vollmer, C. Segel, P. Krooß, J. Günther, L.W. Tseng, I.Karaman, A.Weidner, H. Biermann, T.Niendorf, On the effect of gamma phase formation on the pseudoelastic performance of polycrystalline Fe–Mn–Al–Ni shape memory alloys. Scr. Mater. 108, 23–26 (2015).

[30] S. Takaki, H. Nakatsu, Y. Tokunaga, Effects of austenite grain size on martensitic transformation in Fe15mass%Mn alloys, Mater. Trans. JIM 34 (No.6) (1993) 489-495.

[31] L.M. Guerrero, P. La Roca, F. Malamud, A. Baruj, A. Butera, M. Sade, Strategies to increase austenite FCC relative phase stability in High-Mn steels. J. Alloy. Compd. 854 (2021) 156971.

[32] Seong W. J. , Seong-H. H., Gwang H.L., and Byung D.Y. , Met. Mater. Int., Vol. 19, No. 3 (2013), pp. 585-590.

[33] A. Walnsch, M.J. Kriegel, M. Motylenko et al., Thermodynamics of martensite formation in Fe–Mn–Al–Ni shape memory alloys. Scripta Materialia 192 (2021) 26–31.

[34] Ji Xia, Toshihiro Omori, Ryosuke Kainuma, Abnormal grain growth in Fe–Mn–Al–Ni shape memory alloy with higher Al content, Scripta Materialia 187 (2020) 355–359.